Title:

Tryptophan specialized metabolism and ER body-resident myrosinases modulate root microbiota assembly

Authors:

Arpan Kumar Basak[1,2], Anna Piasecka[3], Jana Hucklenbroich[4], Gözde Merve Türksoy[4], Rui Guan[4,†], Pengfan Zhang[4], Felix Getzke[4], Ruben Garrido-Oter[4,5], Stephane Hacquard[4,5], Kazimierz Strzałka[2,6], Paweł Bednarek[3], Kenji Yamada[2], and Ryohei Thomas Nakano[4*]

Affiliations:

[1]Institute of Environmental Sciences, Faculty of Biology, Jagiellonian University, Krakow, Poland

[2]Malopolska Centre of Biotechnology, Jagiellonian University, Krakow, Poland

[3]Institute of Bioorganic Chemistry, Polish Academy of Sciences, Poznan, Poland

[4]Department of Plant Microbe Interactions, Max Planck Institute for Plant Breeding Research, Cologne, Germany

[5]Cluster of Excellence on Plant Sciences (CEPLAS), Max Planck Institute for Plant Breeding Research, Cologne, Germany

[6]Faculty of Biochemistry, Biophysics and Biotechnology, Department of Plant Physiology and Biochemistry, Jagiellonian University, Krakow, Poland

[†]Present address: The Medical Research Council Toxicology Unit, University of Cambridge, Cambridge, UK

*To whom correspondence may be addressed:

Ryohei Thomas Nakano, Max Planck Institute for Plant Breeding Research, +49(0)221-5062310, nakano@mpipz.mpg.de

The authors declare no conflict of interest.

Classification:

BIOLOGICAL SCIENCES; Plant Biology

Keywords:

Microbiota; Host-microbe interaction; ER body; Glucosinolate; Specialized metabolism; Root exudate

Abstract

Indole glucosinolates (IGs) are tryptophan (Trp)-derived sulfur-containing specialized metabolites that play a crucial role in plant-microbe interactions in plants of the order Brassicales, including *Arabidopsis thaliana*. Despite the growing body of evidence implicating IG biosynthetic pathways in root-microbiota interactions, how myrosinases, the enzymes that convert inert IGs into bioactive intermediate/terminal products, contribute to this process remains unknown. Here, we describe the roles of the PYK10 and BGLU21 myrosinases in root-microbiota assembly partly via metabolites secreted from roots into the rhizosphere. PYK10 and BGLU21 localize to the endoplasmic reticulum (ER) body, an ER-derived organelle observed in plants of the family Brassicaceae. We investigated the root microbiota structure of mutants defective in the Trp metabolic (*cyp79b2b3* and *myb34/51/122*) and ER body (*nai1* and *pyk10bglu21*) pathways and found that these factors together contribute to the assembly of root microbiota. Microbial community composition in soils as well as in bacterial synthetic communities (SynComs) treated with root exudates axenically collected from *pyk10bglu21* and *cyp79b2b3* differed significantly from those treated with exudates derived from wild-type plants, pointing to a direct role of root-exuded compounds. We also show that growth of the *pyk10bglu21* and *cyp79b2b3* mutants was severely inhibited by fungal endophytes isolated from healthy *A. thaliana* plants. Overall, our findings demonstrate that root ER body-resident myrosinases influencing the secretion of Trp-derived specialized metabolites represent a lineage-specific innovation that evolved in Brassicaceae to regulate root microbiota structure.

Significance

ER bodies were first identified in roots of Brassicaceae plants more than 50 years ago, but their physiological functions have remained uncharacterized. A series of previous studies have suggested their possible role in root-microbe interactions. Here, we provide clear experimental

63 evidence showing a role for ER bodies in root-microbiota interactions, which overlaps with that
64 of root-exuded Trp-derived metabolites. Our findings delineate a plant lineage-specific
65 innovation involving intracellular compartments and metabolic enzymes that evolved to regulate
66 plant-microbe interactions at the root-soil interface.
67

INTRODUCTION

ER bodies (Fig 1A; 1) are spindle-shaped organelles that have evolved in plants from taxonomically related families in the order Brassicales, i.e., Brassicaceae, Cleomaceae, and Capparaceae (2, 3). These compartments were originally named "dilated cisternae" upon their discovery using an electron microscope (4), and, since then, a half-century of studies has revealed the molecular nature of these structures. ER bodies in *Arabidopsis thaliana* accumulate large concentrations of β-glucosidase enzymes, PYK10 and BGLU21 in roots/seedlings and BGLU18 in rosette leaves (5-7). A basic helix-loop-helix (bHLH) transcription factor NAI1 controls the formation of ER bodies by positively regulating the expression of genes encoding ER body constituents, including PYK10 and BGLU21, a scaffold protein NAI2, and integral membrane proteins MEMBRANE OF ER BODY 1 (MEB1) and MEB2 (5, 8-13).

ER bodies are constitutively developed in roots and seedlings, while they are strongly induced, both locally and systemically, by wounding or jasmonic acid treatment in mature rosette leaves (7, 14). Recent studies have described the role of leaf ER bodies in defence against herbivores (woodlice), likely mediated by the β-glucosidase (BGLU) activity of PYK10 and BGLU18 (6, 15). In particular, these BGLUs mediate the hydrolysis of glucosinolates (6, 16), a class of specialized metabolites (also known as secondary metabolites) that accumulate in plants of the order Brassicales and that are crucial for defence against herbivores and microbial pathogens (17). The enzymatic capacity to hydrolyse the thioglucosidic bond in glucosinolates is called myrosinase activity and is harboured by only a subset of BGLUs (18). Myrosinase activity toward the tryptophan (Trp)-derived group of glucosinolates with an indole side chain (indole glucosinolates, IG) has been demonstrated for PYK10 and BGLU18 (6, 16), while, *in vitro*, their specific activity towards sinigrin, a short-chain methionine (Met)-derived aliphatic glucosinolate (AG), appears to be lower (5, 19). On the other hand, PYK10 and

BGLU21 can hydrolyse AGs in plant tissue homogenates (15), suggesting that these ER body myrosinases can act on a wide range of glucosinolates. Overall, these studies suggested a role of ER Bodies related to the metabolism of glucosinolates.

In addition to their well-characterized role in restricting pathogenic infection in leaves (20-23), root-accumulating Trp-derived metabolites, including IGs, play a crucial role in interaction with soil-borne non-pathogenic microbes at the root-soil interface (24-28). For example, the *cyp79b2b3* double mutant, in which the major branch of Trp metabolism (the metabolic pathway initiated with a conversion of Trp into indole-3-acetoaldoxime, IAOx) is entirely blocked, is unable to properly manage the accommodation of beneficial endophytic fungi and exhibits severe growth inhibition in the presence of these microbes (25, 27). The *cyp79b2b3* mutant also fails to control the overall abundance of fungi in roots ("fungal load"), resulting in a severe growth defect when inoculated with a synthetic community (SynCom) composed of commensal bacteria and endophytic fungi (28). Notably, Trp-derived specialized metabolites including IG catabolites are reported to be secreted into the rhizosphere (29-31), and an alteration in the profiles of root-produced glucosinolates has an impact on the root-associated bacterial and fungal microbiota (32); whether intact IGs are also secreted along with the IG catabolites appears to be dependent on the investigated species and/or the experimental conditions. Based on these findings, it has been proposed that root ER bodies are involved in plant defence and/or interaction with surrounding microbes via Trp metabolism (16, 33). However, to date, the specific role for the root ER bodies under natural conditions remains unclear.

We hypothesized that the PYK10-mediated hydrolysis of Trp-derived specialized metabolites, including IGs, produces a variety of terminal products and plays an important role in plant-microbiota interactions at the root-soil interface. In this study, we provide evidence that ER bodies and Trp-derived metabolic pathways influence root microbiota composition in an

118 overlapping manner. We also show that this effect on microbial communities is partially
119 mediated by root-exuded compounds and has a direct impact on bacterial community
120 composition in the absence of fungi, as well as on fungal behaviour in the absence of bacteria.
121 Overall, our results demonstrate a physiological role for root ER bodies in shaping root
122 microbiota assembly at the root-soil interface.
123

124 **MATERIALS AND METHODS**

125 **Plant, microbial, and soil materials**

126 Cologne agricultural soil batches 11 (CAS11), 13 (CAS13) and 15 (CAS15) were harvested in
127 February 2017, February 2019, and in January 2020, respectively, as described previously (34).
128 *Arabidopsis thaliana* wild-type Col-0 seeds were obtained from the Nottingham Arabidopsis
129 Stock Centre (NASC). The *pyk10-1 bglu21-1* double mutant (*pyk10bglu21*), *nai1-1*, *myb34*
130 *myb51 myb122* triple mutant (*myb34/51/122*) and *cyp79b2 cyp79b3* double mutant
131 (*cyp79b2b3*) plants have been described previously (5, 35-37). The bacterial and fungal strains
132 used in this study (Table S1 and S2) were described previously (25, 38, 39).
133

134 **Root harvesting and fractionation**

135 After cultivation of plants, roots and soils were harvested from pots and fractionated into
136 rhizosphere, rhizoplane, and endosphere fractions, as described previously (40). Briefly, the
137 soil particles physically attached to the root surface were collected as a rhizosphere fraction by
138 shaking vigorously in sterile water followed by centrifugation. Microbes on the root surface were
139 collected as a rhizoplane fraction by washing roots with detergent followed by filtration through
140 a 0.22-μm membrane. Roots were then surface-sterilized with 70% (v/v) ethanol and bleach
141 solution to give the endosphere fraction. All samples were immediately frozen in liquid nitrogen
142 and stored at -80 °C until processing.

Collection of root exudates

Root exudates were collected from plants hydroponically grown in axenic glass jars containing glass beads, as described previously (41). Seeds of Col-0 wild-type as well as *pyk10bglu21* and *cyp79b2b3* mutant plants were surface-sterilized with 70% (v/v) ethanol and bleach with 12% (w/v) active chlorine and germinated on metal meshes placed on half-strength Murashige and Skoog (MS) basal salts (Sigma-Aldrich), supplemented with 1% (w/v) sucrose and 1% (w/v) agar. Seeds were stratified for 48 hours at 4 ºC in the dark and cultured for four days under short-day conditions (10 hours under light at 21 °C and 14 hours under dark at 19 °C). The four-day-old seedlings on the mesh were transferred aseptically into glass jars containing sterile glass beads (1 mm) and 26 ml of half-strength liquid MS media. Glass jars were placed in a breathable Microbox (Sac O2, Belgium) and cultivated for five weeks under short-day conditions. Hydroponic medium was collected using an aseptic stainless needle into 50-mL tubes and concentrated to 1/10 volume by a lyophilizer.

Metabolite profiling of root exudates

The LC-MS system consisted of UPLC with a photodiode-array detector PDAeλ (Acquity System; Waters) hyphenated with a high-resolution QExactive hybrid MS/MS quadrupole Orbitrap mass spectrometer (Thermo Scientific, http://www.thermofisher.com/). Chromatographic profiles of metabolites and the quantitative measurements were obtained using water acidified with 0.1% formic acid (solvent A) and acetonitrile (solvent B) with a mobile phase flow of 0.35 ml min^{-1} on an ACQUITY UPLC HSS T3 C18 column (2.1 × 50 mm, 1.8 µm particle size; Waters) at 22 °C. The root-exudate sample (5 µL) was injected into the inlet port after purging and rinsing the system. The active MS was operated in Xcalibur version 3.0.63 with the following settings: heated electrospray ionization ion source voltage –3 kV or 3 kV; sheath gas flow 30 L min^{-1}; auxiliary gas flow 13 L min^{-1}; ion source capillary temperature

250 °C; auxiliary gas heater temperature 380 °C. MS/MS mode (data-dependent acquisition) was recorded in negative and positive ionization, in resolution 70000 and AGC (ion population) target 3e+6, scan range 80 to 1000 mz. Obtained LC-MS data were processed for peak detection, deisotoping, alignment and gap-filling by MZmine 2.51 (42) separately for positive and negative ionization mode, then data from both modes were combined. The prepared data table was post-processed for missing values imputation, log transformation and data filtering by MetaboAnalyst (43). Then, data were visualized by Sparse Partial Least Squares Discriminant Analysis and Venn diagrams showing signals selected by one-way ANOVA with Benjamini-Hochberg correction with the following criteria: FDR ≤ 0.05, and | log fold change | ≥ 1.0), where fold change is calculated for specific comparison of *cyp79b2b3* vs Col-0 and *pyk10bglu21* vs Col-0. Glucosinolates were identified based on the MS/MS fragmentation spectra. Standard compounds were used for identification and quantification of IAA, esculetin, fraxetin and scopoletin. Pathway enrichment analysis of the root exudate metabolome was conducted by the MetaboAnalyst modules “Functional Analysis” followed by “Pathway enrichment” on signals selected in previous ANOVA and fold change analysis. Annotation of signals to the KEGG pathway for *A. thaliana* was conducted with a mass tolerance of 5 ppm.

Collection of root extracts

To collect root extracts, we cultured Col-0 wild-type, as well as *pyk10bglu21* and *cyp79b2b3* mutant plants on half-strength MS media, supplemented with 1% (w/v) sucrose and 1% (w/v) agar for 21 days. Roots were weighed, harvested and frozen in liquid nitrogen and stored at -80 ºC until further processing. Immediately before treatment, roots were homogenized in phospho-buffered saline using 1-mm zirconia beads to obtain 10 mg/mL of root extracts.

193 **Soil treatment with root exudates**

194 Approximately 500 mg of CAS soil were transferred into 2 mL screw-cap tubes and treated with
195 50 μL of root exudates or root extracts. Tubes were covered by breathable tape and incubated
196 at 28 °C under dark conditions. Root exudates or freshly prepared root extracts were added
197 every three days to replenish the weight lost due to evaporation of the moisture content. Soils
198 were freeze-dried and stored at -80 °C until further processing.

199

200 **Bacterial microbiota reconstitution experiment**

201 Bacterial cultures were retrieved from glycerol stocks on plates containing 50% (w/v) trypsin
202 soy broth (TSB) supplemented with 1.5% (w/v) agar. Single colonies were used to inoculate
203 50% TSB (15 g/L) liquid media in 96-deep-well plates and cultured for four days at 25 °C. Sixty
204 microlitres of cultures were transferred to another 96-well plate containing 600 μL of the sterile
205 TSB media cultured for another three days in parallel to the original culture plates. Cultures
206 from 7-day-old and 3-day-old plates were pooled and OD_{600} was adjusted to roughly 0.5 for
207 each strain. Individual strains were pooled into a new tube to give a final bacterial concentration
208 of OD_{600} = 1. The bacterial inoculum was centrifuged at 3,000 rpm for 10 minutes to remove
209 the TSB, followed by two washes in 10 mM $MgCl_2$. The obtained pellet was dissolved in $MgCl_2$
210 and OD_{600} was adjusted to 1. The starting inoculum was incubated overnight at 25 ºC, such
211 that bacteria would have consumed nutrients carried over from previous cultures and utilize the
212 root exudate as their sole nutrient source during the treatment. On the day of the SynCom
213 treatment, the concentration of the starting inoculum was adjusted to OD_{600} 0.5. The inoculum
214 was diluted to OD_{600} 0.05 and 0.005 in 50 μl of root exudates. We multiplexed 1,216 samples
215 in two MiSeq runs with barcode sequences in both forward and reverse primers (44) and used
216 a reference-based error correction algorithm (Rbec; 45) to maximize the number of reads used
217 for the quantification of their abundance. At the time of harvest (24 or 72 hours post inoculation;

24 or 72 hpi), a fixed amount of *Escherichia coli* DH5α cells (at final OD_{600} of 0.01 or 0.001 depending on the initial inoculum titre), whose 16S *rRNA* is fully distinguishable from all strains included in our SynCom, was added to each sample to enable quantitative abundance (QA) estimation (46). The harvested cultures were immediately processed for DNA isolation.

DNA extraction and amplicon sequencing

Total DNA from the rhizosphere, rhizoplane and root samples was extracted using the FastDNA SPIN Kit for Soil (MP Biomedicals, Solon, USA), as described previously (40). Bacterial cells in liquid cultures were lysed in alkaline sodium hydroxide and directly used as a PCR template, as described previously (38). The V5–V7 region of bacterial *16S* rRNA gene and the ITS1 region of fungal DNA was PCR-amplified by specific primer sets containing adapter sequences for sequencing and barcode sequences for multiplexing (Tables S3–6). Approximately the same amounts of PCR product were pooled, purified twice using AMPure XP beads (Agencourt) and sequenced by an Illumina MiSeq platform (MiSeq Reagent Kit V3, 600-cycle).

Bioinformatic analysis of microbiome profiling

Pre-processing, demultiplexing and analysis of amplicon sequence variants (ASVs) was performed as described previously (47) using the DADA2 pipeline (48). Taxonomic assignments for ASVs were performed referring to the SILVA (v138) database for bacteria and UNITE (release 04.02.2020; 49) database for fungi. Reference-based analysis of bacterial SynCom data was performed using the Rbec pipeline (45).

Statistical analysis for microbiome profiling

All statistical analyses were performed in R (https://www.r-project.org/). Unconstrained and constrained principal coordinates analyses (PCoA and CPCoA) were performed based on Bray-

Curtis dissimilarities using the cmdscale and capscale functions in the *stats* and *vegan* packages. Differential abundance of ASVs and aggregated ASVs were conducted using the *edgeR* package by fitting relative abundance to a generalized linear model with a negative binomial distribution, controlling for sequencing batch, technical replicates and the experimental batch as random factors.

Plant-fungi binary interaction assay

Fungal inoculation was performed as described previously (24, 39). About 50 mg of fungal mycelium were collected and homogenized in 10 mM $MgCl_2$, which was then used to inoculate surface-sterilized seeds. Plants and fungi were co-cultured on half-strength MS media supplemented with 1% (w/v) agar for 21 days under short-day conditions, and their shoot fresh weights were measured after cultivation.

RESULTS

ER bodies and Trp-derived specialized metabolites together contribute to root microbiota assembly

To investigate the impact of ER bodies and Trp-derived specialized metabolites on root microbiota assembly, we performed amplicon sequencing analysis of bacterial (16S *rRNA*) and fungal (ITS1) microbiota community compositions of *A. thaliana* mutant roots (rhizoplane and endosphere fractions) impaired in ER body-resident myrosinases (*pyk10bglu21*), the formation of ER bodies (*nai1-1*), the biosynthesis of IGs as well as other Trp-derived specialized metabolites to a milder extent (*myb34/51/122*), and the entire specialized Trp metabolism (*cyp79b2b3*), along with the Col-0 wild-type plants (Fig. 1B), grown in natural soils (34). The analysis of β-diversity at the amplicon sequence variant (ASV) level revealed significant differences between the plant genotypes in the bacterial communities in the rhizoplane (P =

0.009; 5.40% of variation explained by genotypes) and in the fungal communities in the endosphere (P = 0.021; 11.41%), while bacterial and fungal communities in the endosphere and rhizoplane, respectively, did not significantly differ across genotypes (Fig 1C; Table S7). Bacterial communities in the rhizoplanes of *cyp79b2b3* and *myb34/51/122* and of *pyk10bglu21* and *nai1* were similar to each other, respectively (Fig 1C; top left), pointing to an active role of IGs and ER bodies in bacterial community assembly rather than a stochastic variation between different host genotypes. On the other hand, in fungal communities, only *cyp79b2b3* and *pyk10bglu21* mutants, in which enzyme-encoding genes were disrupted, showed substantial differences from the wild type, while *myb34/51/122* and *nai1*, the transcription factor mutants, exhibited a milder impact (Fig. 1C; bottom right). This may be explained by Trp-derived metabolites other than IGs accumulating to levels similar to Col-0 and/or residual amounts of IGs and PYK10 and BGLU21 in these mutant roots (9, 22). A similar trend of microbial community shifts in mutants compared to the wild type was observed when we aggregated the relative abundance (RA) of ASVs at the family level (Fig S1); this analysis showed that the observed community shift occurred at the family or higher taxonomic level, rather than at the strain- or species-specific level.

We noted that the bacterial community shift observed in the rhizoplane of mutants compared to the wild type was in the same direction along the first axis, while the ER body mutants and Trp metabolism mutants were separated along the second axis (Fig. 1C; top left). This implied that the loss of ER bodies and Trp-derived metabolites exerted a partly similar impact, if not entirely identical, on the root-associated microbiota structure. This was also supported by the significant positive correlation between the $\log_2$-scale fold changes (logFC) in RA values of ASVs or families between each mutant and wild-type plants (Fig S2 and S3). Namely, bacteria belonging to the families Burkholderiaceae and Oxalobacteraceae/Xanthomonadaceae appeared to be commonly enriched and depleted,

293 respectively, in the mutant rhizoplane compared to the wild type (Fig. S4A). Likewise, fungi
294 belonging to the families Nectriaceae, Plectosphaerellaceae and Cladosporiaceae were found
295 to be commonly enriched in the mutant endosphere compared to the wild type (Fig S4B).
296 Overall, these data demonstrate that the ER body-resident myrosinases and Trp metabolism
297 contribute to microbial community assembly, affecting the behaviour of overlapping sets of
298 microbes.
299
300 **Trp-derived metabolites secreted into the rhizosphere in a manner dependent on PYK10**
301 **and BGLU21 modulate microbiota community structure**
302 The significant bacterial community shift at the rhizoplane (root exterior) suggested a role for
303 root-exuded compounds in bacterial community assembly. To directly test this, we collected
304 root exudates from Col-0 wild-type as well as *pyk10bglu21* and *cyp79b2b3* mutant plants,
305 axenically grown in a hydroponic culture system (41). We first analysed the collected exudates
306 by untargeted HPLC-MS/MS, which revealed a significant difference in the compositions of
307 metabolites between exudates collected from mutants and the wild type (Fig. 2A and Fig S5;
308 Table S8). We observed up to 696 and 1,307 signals with significant differences in their RA
309 values in *pyk10bglu21* and/or *cyp79b2b3* root exudates compared to Col-0 exudates, among
310 which 34 and 273 signals were commonly depleted/enriched in both mutant exudates (Fig. 2B
311 and Table S9). This result demonstrates that Trp-derived specialized metabolites are indeed
312 secreted to the rhizosphere, and PYK10 and BGLU21 either directly or indirectly contribute to
313 the secretion of these metabolites as well as other metabolites.
314 Given the major variation between experimental batches, while the overall tread was
315 similar, we decided to focus on one batch of exudate samples for further experiments. We
316 treated natural soils with these different root exudates and analysed their impact on soil
317 bacterial and fungal community structures (Fig. 3A). We found that, after 15 days of consecutive

318 treatments with 2-day intervals, the soil microbial communities exhibited a shift compared to
319 those from mock-treated soils, which is consistent with a previous study (50), in a manner
320 dependent on the genotypes of origin of the root exudates (Fig. 3A; middle panels). Both
321 bacterial and fungal communities in the soils treated with *pyk10bglu21* or *cyp79b2b3* exudates
322 were significantly different from each other and from the communities in the soils treated with
323 Col-0 exudates. Microbial taxa exhibiting differential abundance in soils treated with mutant and
324 Col-0 root exudates were largely similar between *pyk10bglu21* and *cyp79b2b3*, (Fig S6A), and
325 the logFC in their RA values relative to the wild-type controls were positively correlated between
326 *pyk10bglu21* and Col-0 and *cyp79b2b3* and Col-0, both at the ASV and the family levels (Fig.
327 3A; right panel).

328 PYK10 and BGLU21 are stored in ER bodies and do not encounter with their potential
329 substrates in other subcellular compartments, such as vacuoles (33). Next, to test whether
330 PYK10 and BLGLU21 contribute to the secretion of metabolites responsible for the observed
331 community shifts or their accumulation in roots, we prepared axenic root crude extracts from
332 these genotypes and performed the same soil treatment experiment (Fig. 3B; Table S9). The
333 root extract treatments also triggered significant community shifts in the soil microbial
334 community compared to mock-treated soils (Fig. 3B; middle panels). Interestingly, the
335 constrained PCoA plots showed that Col-0 and *pyk10bglu21* root extracts triggered similar
336 shifts in the microbial community compositions, while treatments with *cyp79b2b3* root extracts
337 resulted in significantly different community structures. Comparison of logFC in RA values of
338 ASVs and families also pointed to the presence of a group of microbes that were specifically
339 affected by the CYP79B2 and CYP79B3 pathway but not by the PYK10 and BGLU21 pathway
340 (Fig 3B, right panel; Fig S6B). These findings suggest that the Trp-derived metabolites
341 responsible for the community assembly when treated with the Col-0 root extracts are not
342 secreted into the rhizosphere but in fact accumulate in the *pyk10bglu21* roots. *A. thaliana* roots

accumulate many myrosinases that are not stored in ER bodies, such as TGG4, TGG5, and PEN2 (51, 52), which are capable of catalysing the same reaction as PYK10 and BGLU21 when subcellular membrane partitions are artificially disrupted in a homogenate. Therefore, the active compounds may be accumulated in *pyk10bglu21* roots either in an already active form or in an inactive glycosylated form. Overall, these results suggest a role for Trp-derived metabolites whose secretion but not accumulation is dependent on ER body myrosinases in modulating microbial community structures.

Root-exuded compounds directly affect bacterial community structure independently of fungi

Trp-derived metabolites, including IGs, have been reported to be crucial for interaction with endophytic fungi (25, 28), while their impact on bacteria remains less understood. To assess the direct impact of root exudates on bacterial community assembly, we performed a synthetic community (SynCom) profiling experiment in these root exudates (Fig. 4A), using 171 bacterial strains isolated from healthy *A. thaliana* roots grown in natural soil and 29 strains isolated from the same, unplanted soil (38). The analysis of β-diversity based on RA values revealed that the SynCom compositions in the Col-0 root exudates were significantly different from the composition in the mutant root exudates (Fig. 4B; Table S10). The effect on bacterial community composition was more different between Col-0 and *cyp79b2b3* exudates than between Col-0 and *pyk10bglu21* exudates, which is similar to what was observed in the soil treatment experiment (Fig. 3). The community shift in mutants compared to Col-0 was significant with both initial titres (OD_{600} of 0.05 and 0.005) and at both time points (24 and 72 hpi). The overall variance explained by genotypes was larger when we used a lower titre as a starting inoculum, and we observed a higher level of overall community growth (increase in the total number of bacterial cells within the community measured by the quantitative abundance normalized to *E.*

coli cells spiked in before DNA extraction) under the low-titre than high-titre conditions, while between genotypes, the overall community growth was largely similar (Fig. S7A). When we compared the community structure dynamics over time within genotypes, we observed a more dynamic community assembly at 24 hpi when we used low-titre inocula, with eventual convergence on a similar community structure at 72 hpi (Fig. S7B). These data suggest that the contribution of ER bodies and Trp-derived specialized metabolites to community assembly is larger when bacterial cells are metabolically more active and undergoing dynamic community re-assembly. We compared the growth of each bacterial strain in Col-0 and mutant exudates (Fig. S7C) and found a small group of strains that showed a similar response in mutant exudates in comparison to Col-0 exudates (Fig. S7D), pointing to a set of bacteria commonly targeted by these pathways via root-exuded compounds. Overall, these results suggest that Trp-derived metabolites secreted to the rhizosphere in a PYK10 and BGLU21-dependent manner can directly impact the bacterial community assembly in the absence of eukaryotic organisms, such as plants and fungi.

ER bodies and Trp-derived metabolites directly influence plant-fungus interactions

Lastly, we tested whether the ER body pathway and the Trp metabolic pathway have a direct impact also on the plant-fungus interaction in the absence of bacteria. Toward this end, we inoculated the same set of plants (Col-0, *pyk10bglu21*, and *cyp79b2b3*) in a mono-association setup (24; Fig. 5) with fungal strains isolated from roots or leaves of healthy *A. thaliana* and related species grown in natural soils (25, 39). We found that the growth of *cyp79b2b3* mutant plants was severely impaired by more than half of the strains compared to the wild-type plants (24 isolates), especially by those belonging to the classes Leothiomycetes and Dothideomycetes. Furthermore, seven strains were found to significantly impair the growth of both *cyp79b2b3* and *pyk10bglu21* mutants compared to Col-0. On the other hand, 16 isolates,

including all those belonging to the class Leotiomycetes, specifically restricted the growth of *cyp79b2b3* but not *pyk10bglu21* plants, and three strains showed a negative impact only on *pyk10bglu21* compared to the Col-0 wild type. These results demonstrate that the myrosinases stored in ER bodies and Trp-derived metabolites directly regulate plant-fungus interactions and target distinct but overlapping sets of fungal strains. Combined with the results that the ER body and Trp-derived metabolic pathways together contribute to the bacterial and fungal community assembly at the rhizoplane and in the endosphere, respectively, our overall findings illustrate a role for ER body-resident myrosinase-mediated Trp metabolism in root-microbiota interactions.

DISCUSSION

The role of ER bodies and Trp-derived metabolites in root-microbiota interactions

Here, we have provided clear evidence supporting the idea that the ER body and the myrosinases that accumulate therein are involved in root-microbiota interactions, and the effects of the loss of ER body myrosinases were partly similar to the effects of the loss of Trp metabolism. This strongly suggests that there is link between ER bodies and Trp-derived compounds in interaction with soil-borne microbes. Trp metabolism produces non-glycosylated metabolites, such as camalexin and indol-3-carbonyl nitriles, and PYK10 and BGLU21 can hydrolyse glucosides derived from other amino acids, such as AGs from Met and coumarin glucosides from phenylalanine. Our pathway enrichment analysis of differentially abundant metabolites in our root exudate samples, based on the KEGG annotations of metabolites, identified biosynthetic pathways of phenylpropanoids, flavonoids and terpenoids (Table S8), without a clear commonality between *pyk10blu21* and *cyp79b2b3* exudates, further supporting the idea that the substrates of PYK10 and BGLU21 are not limited to Trp-derived glucosides. Therefore, it is plausible that the specific effects observed in each of the *pyk10bglu21* and *cyp79b2b3* mutants were due to an impaired production and/or secretion of these specific

418 metabolites, while the common effect can be attributed to the Trp-derived glucosides, such as
419 IGs, and their catabolites.

420 Of note, our metabolomic analysis of root exudates clearly indicates that PYK10 and
421 BGLU21 contribute to the secretion of specialized metabolites, including but not limited to those
422 derived from Trp (Fig. 2, Fig. S5, and Table S8; discussed below). This suggests that the
423 enzymes *intracellularly* stored in ER bodies influence the composition of specialized
424 metabolites that are *extracellularly* exuded from roots into the rhizosphere. A plausible scenario
425 is that PYK10 and BGLU21 mediate conversion of glycosylated metabolites into a form that can
426 be secreted into the rhizosphere, which has been reported in other plant specialized
427 metabolites. For instance, secretion of scopoletin into the rhizosphere is severely restricted by
428 genetic disruption of BGLU42, which is a cytosolic enzyme capable of removing the glucose
429 moiety from scopolin, the glucosidic form of scopoletin, ultimately affecting the root-associated
430 microbiota structure (53). We speculate that PYK10- and BGLU21-mediated removal of a
431 glucose moiety from Trp-derived glycosylated compounds plays a role in the secretion of
432 respective aglycones or their catabolites. Alternatively, it also remains possible that a part of
433 PYK10 and BGLU21 proteins are secreted to the apoplast or deposited to the rhizoplane
434 through the secretory pathway from the ER, thereby metabolizing the glucosides secreted from
435 root tissues.

436 Despite the finding that the lack of PYK10 and BGLU21 showed a larger impact on the
437 metabolomic profile of root exudates than the lack of the entire Trp metabolism (Fig. 2A), the
438 impact on soil microbial community triggered by the lack of Trp metabolism was larger than
439 what was triggered by the lack of these myrosinases. This suggests that, while PYK10 and
440 BGLU21 are involved in the secretion of a wide range of metabolites under axenic conditions,
441 a fraction of these compounds, plausibly those derived from Trp, has the predominant role in
442 shaping the root-associated microbial community assembly.

Possible role of IGs and IG catabolites and ER body myrosinases in root-associated microbiota assembly

Trp-derived specialized metabolites are crucial for plant-microbe interactions, and their role in plant-microbiota interactions has been well described. For example, a recent work identified a fungal dysbiosis phenotype (increased fungal load in roots) of *cyp79b2b3*, resulting in a severe plant growth defect in the presence of fungal endophytes (28). This fungal dysbiosis phenotype was not observed in the *myb34/51/122* mutant roots or in any known mutants in the Trp-derived branch pathways, pointing to the presence of uncharacterized metabolites that are crucial for regulating the fungal load in roots. In this study, we observed a significant alteration in the bacterial and fungal communities in roots of *myb34/51/122*, which is specifically impaired in IG biosynthesis but retains the ability to produce other Trp-derived metabolites (35), indicating that IGs also play a role in root-microbiota interactions. On the other hand, we did not detect substantial amounts of intact IGs in the root exudates, even those collected from Col-0 wild-type plants (Figure S5L-N), which is consistent with what was reported in a previous study employing a similar experimental approach (30). Low levels of IGs in root exudates could be due to rapid degradation of IGs after root secretion by an uncharacterized extracellular myrosinase or a requirement for glucose removal for secretion of IG catabolites. Alternatively, it is also possible that IGs and their catabolites are secreted at lower levels than expected from axenic and naïve plants under our experimental conditions without any immuno-stimuli, as an activation of immune responses by microbe-associated molecular patterns (MAMPs) induces secretion of Trp-derived metabolites including camalexin (26). Because several IG catabolites, such as isothiocyanates and carbinols, are unstable and difficult to detect, and our understanding of other stable IG catabolites remains limited, it remains to be determined whether IGs and IG catabolites are secreted but not detected or whether these compounds are not secreted in substantial amounts into the rhizosphere.

Auxin and other Trp-derived metabolites can be secreted in an ER body myrosinase-dependent manner and contribute to bacterial community assembly

Our data also do not exclude the possibility that PYK10 and BGLU21 influence secretion of Trp-derived metabolites other than IGs that play a key role in manipulating microbial community composition. We detected a variety of Trp-derived specialized metabolites in our exudate samples, such as indole-3-acetic acid (IAA), indole-3-acetonitrile (IAN) and indole-3-carboxylic acid (ICA) (Fig. S5). Of note, the RA values of IAA in exudates collected from *pyk10bglu21* and *cyp79b2b3* mutant roots were lower than in exudates from Col-0 roots ($P < 0.001$ for *cyp79b2b3* vs Col-0; $P = 0.0516$ for *pyk10bglu21*), and a similar trend was observed in IAN (Fig. S5). Trp metabolism is initiated with oxidation of Trp by CYP79B2 and CYP79B3, producing IAOx as a product. IAOx is further oxidized to IAN or 1-aci-nitro-2-indolyl-ethane by CYP71A12 and CYP71A13 or CYP83B1, respectively, which are the precursors of camalexin and IGs, respectively. IAN can also be a substrate for a group of nitrilases that directly produce IAA (54), which is one of the multiple Trp-derived IAA biosynthetic pathways (37). Importantly, IAN can also be produced as a terminal product of IG catabolic processes mediated by myrosinases, and a recent simulation modelling study suggested that plants can alter IAA signalling dynamics following the hydrolysis of IGs in a manner dependent on the responsible IG-hydrolysing myrosinases (55). Therefore, it is plausible that the hydrolysis of IGs by PYK10 and BGLU21 contributes to the secretion of IAA into the rhizoplane/rhizosphere. Auxin, including IAA, by itself has an impact on microbial behaviour (56, 57), and root-associated commensal bacteria are capable of modulating auxin accumulation in roots (58). Overall, these data raise the possibility that modulation of the microbial community by root exudates is partly accounted for by auxin and that the root secretion of auxin is directly or indirectly dependent on the myrosinase activity of PYK10 and BGLU21.

It is also important to note that the exudates used in our experiments were collected from axenic, naïve plants, i.e., in the absence of microbes or any immune elicitors. It has been well described that plant immune status has an impact on root metabolomic profiles (26, 52) as well as on root exudation profiles (59-61). It is therefore likely that the metabolomic profile of root exudates may be substantially different between axenic and soil conditions. Our results nonetheless provide evidence that Trp-derived metabolites that are secreted in a manner dependent on PYK10 and BGLU21 under axenic naïve conditions, including IAA and IAN, are capable of manipulating a microbial community; further studies will address to which extent our insights into the activity of axenic root exudates can explain the actual microbial community shift observed in the greenhouse experiment (Fig. 1).

Root-produced glucosides might represent a general plant strategy to shape the soil-borne microbiome

Glucosinolates and ER bodies are specifically found in plants within the order Brassicales and represent lineage-specific innovations of plant secondary metabolism and its regulation, respectively. While IGs are conserved across the entire order (62), the ER body system appears to be a more recent innovation, arising approximately between 50 and 60 million years ago (63), just before separation of Brassicacaee, Capparaceae, and Cleomaceae from the other Brassicales (64). This suggests that ER bodies contribute to boosting the overall efficacy of the IG-mediated defence system. Such lineage-specific innovation of glucosides that are important for plant-microbe interactions appears to be a common feature of plants. For instance, benzoxazinoids in maize are crucial for rhizosphere microbiota assembly (65), and benzoxazinoids are also produced and accumulate as glucosides that are activated by the action of respective BGLUs (66). The role of benzoxazinoids in plant-soil feedback indicates the involvement of root exudates; whether it is benzoxazinoids or their glycosylated forms that

are secreted into soil remains unclear. Glycosylation of bioactive specialized metabolites to avoid autotoxicity appears to be a common strategy for plants, which enables rapid responses to environmental cues, such as pathogenic/herbivorous invasion (67). Of note, it is proposed that glucosinolates arose from cyanogenic glycosides, which are also important for anti-microbial defence (68) and undergo very similar metabolic processing during their activation, including hydrolytic deglycosylation by cyanogenic BGLUs and detoxification by glutathione conjugation (69). Given the toxicity of HCN that is formed during the deglycosylation of cynogenic glucosides, it is possible that cyanogenic glycosides are also involved in root microbiota assembly. Together with the fact that BGLU activity is needed for secretion of scopoletin into the rhizosphere via removal of glucose from its glycosylated from, scopolin (70), glucose conjugation may be important not only for suppression of toxicity but also to control secretion processes. Based on these insights, we propose that root microbiota assembly mediated by root-produced glucosides and the facilitation of their bioactivity and/or their secretion by cognate BGLUs is a widespread strategy in plants to modulate root microbiota compositions, albeit exploiting different classes of glucosides depending on the plant lineages.

Data Availability

The raw sequences are available at the European Nucleotide Archive (ENA) under the accession number PRJEB54088. The scripts used for processing the Illumina reads and statistical analyses are available at https://github.com/Guan06/DADA2_pipeline and https://github.com/arpankbasak/ERBody_RootMicrobiota.

Supplementary data

Figure S1. Community shifts observed in the mutant roots compared to Col-0 roots retained at the family level.

Figure S2. Similar effects of ER body pathway and Trp metabolism on root microbiota community structure at the ASV level.

Figure S3. Similar effects of ER body pathway and Trp metabolism on root microbiota community structure at the family level.

Figure S4. Several bacterial and fungal families are commonly enriched or depleted in mutant roots compared to wild-type roots.

Figure S5. Composition of specialized metabolites differing within the mutant root exudates.

Figure S6. The relative abundance of microbes is different in the mutant root compartment compared to the wild type.

Figure S7. Community dynamics and growth of individual microbes in a SynCom treated with root exudates.

Table S1. List of bacterial strains used in the SynCom.

Table S2. List of fungal strains used in the mono-association assay.

Table S3. Barcoded primers used for bacterial 16s V5–V7 amplicon sequencing.

Table S4. Barcoded primers used for bacterial ITS1 amplicon sequencing.

Table S5. Forward barcoded primer set for bacterial 16s V5–V7 amplicon sequencing.

Table S6. Forward barcoded primer set for bacterial ITS1 amplicon sequencing.

Table S7. Summary statistics of community structure analysis by constrained ordination followed by pairwise PERMANOVA for the greenhouse experiment.

Table S8. Summary pathway enrichment analysis of root exudate metabolome.

Table S9. Summary statistics of community structure analysis by constrained ordination followed by pairwise PERMANOVA for the soil treatment experiment.

Table S10. Summary statistics of community structure analysis by constrained ordination followed by pairwise PERMANOVA for the SynCom experiment.

Acknowledgements

We thank Paul Schulze-Lefert for providing all necessary infrastructures and instrumentation at the Max Planck Institute for Plant Breeding Research, as well as Małopolska Centre of Biotechnology, Jagiellonian University, for their institutional support. We are grateful to Anna Lisa Roth, Brigitte Pickel, Dieter Becker and Diana Dresbach for their technical support and to Kathrin Wippel, Paloma Durán, and Tomohisa Shimasaki for their technical help in the hydroponic culture, community profiling and soil treatment experiments, respectively. We thank Neysan Donnelly for their help in editing the manuscript.

Funding

This work was supported by an Overseas Research Fellowship funded by the Japanese Society for the Promotion of Science (JSPS) to R.T.N., the Priority Programme "Reconstruction and Deconstruction of Plant Microbiota" (DECRyPT) [402201269] funded by the Deutsche Forschungsgemeinschaft (DFG) to R.T.N., the National Science Centre of Poland grants OPUS [UMO-2016/23/B/NZ1/01847] to A.K.B. and K.Y. and HARMONIA [UMO-2015/18/M/NZ1/00406] to P.B.

References

1. R. Matsushima *et al.*, The ER Body, a Novel Endoplasmic Reticulum-Derived Structure in Arabidopsis. *Plant and Cell Physiology* **44**, 661-666 (2003).
2. I. Hara-Nishimura, R. Matsushima, A wound-inducible organelle derived from endoplasmic reticulum: a plant strategy against environmental stresses? *Current Opinion in Plant Biology* **6**, 583-588 (2003).
3. Y. Hayashi *et al.*, A Proteinase-Storing Body that Prepares for Cell Death or Stresses in the Epidermal Cells of Arabidopsis. *Plant and Cell Physiology* **42**, 894-899 (2001).
4. H. T. Bonnett, E. H. Newcomb, Polyribosomes and cisternal accumulations in root cells of radish. *Journal of Cell Biology* **27**, 423-432 (1965).
5. R. Matsushima, M. Kondo, M. Nishimura, I. Hara-Nishimura, A novel ER-derived compartment, the ER body, selectively accumulates a beta-glucosidase with an ER-retention signal in Arabidopsis. *Plant J* **33**, 493-502 (2003).
6. A. Nakazaki *et al.*, Leaf Endoplasmic Reticulum Bodies Identified in Arabidopsis Rosette Leaves Are Involved in Defense against Herbivory. *Plant Physiol* **179**, 1515-1524 (2019).
7. K. Ogasawara *et al.*, Constitutive and Inducible ER Bodies of *Arabidopsis thaliana* Accumulate Distinct β-Glucosidases. *Plant and Cell Physiology* **50**, 480-488 (2009).
8. A. K. Basak, M. Mirzaei, K. Strzalka, K. Yamada, Texture feature extraction from microscope images enables a robust estimation of ER body phenotype in Arabidopsis. *Plant Methods* **17**, 109 (2021).
9. R. Matsushima, Y. Fukao, M. Nishimura, I. Hara-Nishimura, *NAI1* Gene Encodes a Basic-Helix-Loop-Helix–Type Putative Transcription Factor That Regulates the Formation of an Endoplasmic Reticulum–Derived Structure, the ER Body. *Plant Cell* **16**, 1536-1549 (2004).
10. K. Yamada, A. J. Nagano, M. Nishina, I. Hara-Nishimura, M. Nishimura, NAI2 Is an Endoplasmic Reticulum Body Component That Enables ER Body Formation in *Arabidopsis thaliana*. *Plant Cell* **20**, 2529-2540 (2008).
11. K. Yamada, A. J. Nagano, M. Nishina, I. Hara-Nishimura, M. Nishimura, Identification of two novel endoplasmic reticulum body-specific integral membrane proteins. *Plant Physiology* **161**, 108-120 (2013).
12. S. Sarkar, N. Stefanik, T. Kunieda, I. Hara-Nishimura, K. Yamada, The Arabidopsis transcription factor NAI1 activates the NAI2 promoter by binding to the G-box motifs. *Plant Signal Behav* **16**, 1846928 (2021).
13. N. Stefanik *et al.*, NAI2 and TSA1 Drive Differentiation of Constitutive and Inducible ER Body Formation in Brassicaceae. *Plant Cell Physiol* **61**, 722-734 (2020).
14. R. Matsushima *et al.*, An Endoplasmic Reticulum-Derived Structure That Is Induced under Stress Conditions in Arabidopsis. *Plant Physiology* **130**, 1807-1814 (2002).
15. K. Yamada *et al.*, Endoplasmic reticulum-derived bodies enable a single-cell chemical defense in Brassicaceae plants. *Commun Biol* **3**, 21 (2020).
16. R. T. Nakano *et al.*, PYK10 myrosinase reveals a functional coordination between endoplasmic reticulum bodies and glucosinolates in Arabidopsis thaliana. *Plant J* **89**, 204-220 (2017).
17. U. Wittstock, B. A. Halkier, Glucosinolate research in the Arabidopsis era. *Trends Plant Sci* **7**, 263-270 (2002).

18. W. P. Burmeister *et al.*, The crystal structures of *Sinapis alba* myrosinase and a covalent glycosyl enzyme intermediate provide insights into the substrate recognition and active-site machinery of an *S*-glycosidase. *Structure* **5**, 663-676 (1997).
19. Y. O. Ahn *et al.*, Scopolin-hydrolyzing β-glucosidases in roots of *Arabidopsis*. *Plant and Cell Physiology* **51**, 132-143 (2010).
20. P. Bednarek *et al.*, A Glucosinolate Metabolism Pathway in Living Plant Cells Mediates Broad-Spectrum Antifungal Defense. *Science* **323**, 101-106 (2009).
21. N. K. Clay, A. M. Adio, C. Denoux, G. Jander, F. M. Ausubel, Glucosinolate Metabolites Required for an *Arabidopsis* Innate Immune Response. *Science* **323**, 95-101 (2009).
22. H. Frerigmann *et al.*, Regulation of Pathogen-Triggered Tryptophan Metabolism in Arabidopsis thaliana by MYB Transcription Factors and Indole Glucosinolate Conversion Products. *Molecular Plant* **9**, 682-695 (2016).
23. K. Hiruma *et al.*, Entry Mode-Dependent Function of an Indole Glucosinolate Pathway in Arabidopsis for Nonhost Resistance against Anthracnose Pathogens. *Plant Cell* **22**, 2429-2443 (2010).
24. H. Frerigmann, M. Piotrowski, R. Lemke, P. Bednarek, P. Schulze-Lefert, A Network of Phosphate Starvation and Immune-Related Signaling and Metabolic Pathways Controls the Interaction between Arabidopsis thaliana and the Beneficial Fungus Colletotrichum tofieldiae. *Molecular Plant-Microbe Interactions* **34**, 560-570 (2021).
25. K. Hiruma *et al.*, Root Endophyte Colletotrichum tofieldiae Confers Plant Fitness Benefits that Are Phosphate Status Dependent. *Cell* **165**, 464-474 (2016).
26. A. Koprivova *et al.*, Root-specific camalexin biosynthesis controls the plant growth-promoting effects of multiple bacterial strains. *Proceedings of the National Academy of Sciences of the United States of America* **116**, 15735-15744 (2019).
27. U. Lahrmann *et al.*, Mutualistic root endophytism is not associated with the reduction of saprotrophic traits and requires a noncompromised plant innate immunity. *New Phytol* **207**, 841-857 (2015).
28. K. W. Wolinska *et al.*, Tryptophan metabolism and bacterial commensals prevent fungal dysbiosis in Arabidopsis roots. *Proc Natl Acad Sci U S A* **118** (2021).
29. M. Schreiner, A. Krumbein, D. Knorr, I. Smetanska, Enhanced Glucosinolates in Root Exudates of Brassica rapa ssp rapa Mediated by Salicylic Acid and Methyl Jasmonate. *Journal of Agricultural and Food Chemistry* **59**, 1400-1405 (2011).
30. N. Strehmel, C. Bottcher, S. Schmidt, D. Scheel, Profiling of secondary metabolites in root exudates of Arabidopsis thaliana. *Phytochemistry* **108**, 35-46 (2014).
31. D. Y. Xu *et al.*, Rhizosecretion of stele-synthesized glucosinolates and their catabolites requires GTR-mediated import in Arabidopsis. *Journal of Experimental Botany* **68**, 3205-3214 (2017).
32. M. Bressan *et al.*, Exogenous glucosinolate produced by Arabidopsis thaliana has an impact on microbes in the rhizosphere and plant roots. *Isme Journal* **3**, 1243-1257 (2009).
33. R. T. Nakano, K. Yamada, P. Bednarek, M. Nishimura, I. Hara-Nishimura, ER bodies in plants of the Brassicales order: Biogenesis and association with innate immunity. *Frontiers in Plant Science* **5** (2014).
34. D. Bulgarelli *et al.*, Revealing structure and assembly cues for Arabidopsis root-inhabiting bacterial microbiota. *Nature* **488**, 91-95 (2012).
35. H. Frerigmann, T. Gigolashvili, MYB34, MYB51, and MYB122 distinctly regulate indolic glucosinolate biosynthesis in Arabidopsis thaliana. *Mol Plant* **7**, 814-828 (2014).
36. A. J. Nagano *et al.*, Quantitative Analysis of ER Body Morphology in an *Arabidopsis* Mutant. *Plant and Cell Physiology* **50**, 2015-2022 (2009).

37. Y. D. Zhao *et al.*, Trp-dependent auxin biosynthesis in Arabidopsis: involvement of cytochrome P450s CYP79B2 and CYP79B3. *Genes & Development* **16**, 3100-3112 (2002).
38. Y. Bai *et al.*, Functional overlap of the Arabidopsis leaf and root microbiota. *Nature* **528**, 364-+ (2015).
39. F. Mesny *et al.*, Genetic determinants of endophytism in the Arabidopsis root mycobiome. *Nature Communications* **12** (2021).
40. P. Duran *et al.*, Microbial Interkingdom Interactions in Roots Promote Arabidopsis Survival. *Cell* **175**, 973-+ (2018).
41. K. Wippel *et al.*, Host preference and invasiveness of commensal bacteria in the Lotus and Arabidopsis root microbiota. *Nature Microbiology* **6**, 1150-+ (2021).
42. T. Pluskal, S. Castillo, A. Villar-Briones, M. Oresic, MZmine 2: Modular framework for processing, visualizing, and analyzing mass spectrometry-based molecular profile data. *Bmc Bioinformatics* **11** (2010).
43. Z. Q. Pang *et al.*, MetaboAnalyst 5.0: narrowing the gap between raw spectra and functional insights. *Nucleic Acids Research* **49**, W388-W396 (2021).
44. F. Getzke, S. Hacquard, High-Throughput Profiling of Root-Associated Microbial Communities. *Methods Mol Biol* **2494**, 325-337 (2022).
45. P. Zhang, S. Spaepen, Y. Bai, S. Hacquard, R. Garrido-Oter, Rbec: a tool for analysis of amplicon sequencing data from synthetic microbial communities. *ISME Communications* **1**, 73 (2021).
46. D. S. Lundberg *et al.*, Host-associated microbe PCR (hamPCR) enables convenient measurement of both microbial load and community composition. *Elife* **10** (2021).
47. C. J. Harbort *et al.*, Root-Secreted Coumarins and the Microbiota Interact to Improve Iron Nutrition in Arabidopsis. *Cell Host & Microbe* **28**, 825-+ (2020).
48. B. J. Callahan *et al.*, High-throughput amplicon sequencing of the full-length 16S rRNA gene with single-nucleotide resolution. *Nucleic Acids Research* **47** (2019).
49. R. H. Nilsson *et al.*, The UNITE database for molecular identification of fungi: handling dark taxa and parallel taxonomic classifications. *Nucleic Acids Research* **47**, D259-D264 (2019).
50. D. V. Badri, J. M. Chaparro, R. F. Zhang, Q. R. Shen, J. M. Vivanco, Application of Natural Blends of Phytochemicals Derived from the Root Exudates of Arabidopsis to the Soil Reveal That Phenolic-related Compounds Predominantly Modulate the Soil Microbiome. *Journal of Biological Chemistry* **288**, 4502-4512 (2013).
51. L. L. Fu *et al.*, Arabidopsis Myrosinase Genes AtTGG4 and AtTGG5 Are Root-Tip Specific and Contribute to Auxin Biosynthesis and Root-Growth Regulation. *International Journal of Molecular Sciences* **17** (2016).
52. Y. A. Millet *et al.*, Innate Immune Responses Activated in Arabidopsis Roots by Microbe-Associated Molecular Patterns. *Plant Cell* **22**, 973-990 (2010).
53. I. A. Stringlis *et al.*, MYB72-dependent coumarin exudation shapes root microbiome assembly to promote plant health. *Proceedings of the National Academy of Sciences of the United States of America* **115**, E5213-E5222 (2018).
54. J. Normanly, P. Grisafi, G. R. Fink, B. Bartel, Arabidopsis mutants resistant to the auxin effects of indole-3-acetonitrile are defective in the nitrilase encoded by the NIT1 gene. *Plant Cell* **9**, 1781-1790 (1997).
55. D. Vik, N. Mitarai, N. Wulff, B. A. Halkier, M. Burow, Dynamic Modeling of Indole Glucosinolate Hydrolysis and Its Impact on Auxin Signaling. *Frontiers in Plant Science* **9** (2018).

56. A. T. Djami-Tchatchou *et al.*, Dual Role of Auxin in Regulating Plant Defense and Bacterial Virulence Gene Expression During Pseudomonas syringae PtoDC3000 Pathogenesis. *Molecular Plant-Microbe Interactions* **33**, 1059-1071 (2020).
57. E. Tzipilevich, D. Russ, J. L. Dangl, P. N. Benfey, Plant immune system activation is necessary for efficient root colonization by auxin-secreting beneficial bacteria. *Cell Host & Microbe* **29**, 1507-+ (2021).
58. O. M. Finkel *et al.*, A single bacterial genus maintains root growth in a complex microbiome. *Nature* **587**, 103-+ (2020).
59. D. V. Badri, J. M. Vivanco, Regulation and function of root exudates. *Plant Cell and Environment* **32**, 666-681 (2009).
60. P. Bednarek, B. Schneider, A. Svatos, N. J. Oldham, K. Hahlbrock, Structural complexity, differential response to infection, and tissue specificity of indolic and phenylpropanoid secondary metabolism in *Arabidopsis* roots. *Plant Physiology* **138**, 1058-1070 (2005).
61. A. Koprivova, V. Volz, S. Kopriva, Shoot-root interaction in control of camalexin exudation in Arabidopsis. *bioRxiv* 10.1101/2020.12.15.422875, 2020.2012.2015.422875 (2020).
62. N. Agerbirk *et al.*, Comparison of glucosinolate diversity in the crucifer tribe Cardamineae and the remaining order Brassicales highlights repetitive evolutionary loss and gain of biosynthetic steps. *Phytochemistry* **185** (2021).
63. P. P. Edger *et al.*, The butterfly plant arms-race escalated by gene and genome duplications. *Proc Natl Acad Sci U S A* **112**, 8362-8366 (2015).
64. L. B. Jørgensen, Myrosin cells and dilated cisternae of the endoplasmic reticulum in the order Capparales. *Nordic Journal of Botany* **1**, 433-445 (1981).
65. L. F. Hu *et al.*, Root exudate metabolites drive plant-soil feedbacks on growth and defense by shaping the rhizosphere microbiota. *Nature Communications* **9** (2018).
66. D. Sicker, M. Frey, M. Schulz, A. Gierl, Role of natural benzoxazinones in the survival strategy of plants. *Int Rev Cytol* **198**, 319-346 (2000).
67. S. Pentzold, M. Zagrobelny, P. S. Roelsgaard, B. L. Moller, S. Bak, The Multiple Strategies of an Insect Herbivore to Overcome Plant Cyanogenic Glucoside Defence. *Plos One* **9** (2014).
68. A. O. Ubalua, Cyanogenic Glycosides and the fate of cyanide in soil. *Aust J Crop Sci* **4**, 223-237 (2010).
69. R. M. Gleadow, B. L. Moller, Cyanogenic Glycosides: Synthesis, Physiology, and Phenotypic Plasticity. *Annual Review of Plant Biology, Vol 65* **65**, 155-185 (2014).
70. C. Zamioudis, J. Hanson, C. M. J. Pieterse, β-Glucosidase BGLU42 is a MYB72-dependent key regulator of rhizobacteria-induced systemic resistance and modulates iron deficiency responses in Arabidopsisroots. *New Phytologist* papers2://publication/doi/10.1111/nph.12980, n/a-n/a (2014).

Main Figure legends

Figure 1. ER bodies and Trp metabolism play a role in root-associated microbiota assembly. (*A*) Roots of *A. thaliana* developing a large amount of ER bodies, visualized by ER-localized GFP (SP-GFP-HDEL). Cell wall was stained by propidium iodide. The bar corresponds to 50 μm. (*B*) Representation of IG biosynthetic and catabolic pathways. Arrows and dotted arrows indicate metabolic reactions and transcriptional regulation, respectively. (*C*) Constrained principal coordinates analysis (PCoA) of the bacterial and fungal community structures in the roots of Col-0 as well as mutants impaired in ER body formation (*nai1-1*), ER body-accumulating myrosinases (*pyk19bglu21*), IG biosynthesis (*myb34/51/122*), and Trp metabolism (*cyp79b2b3*) based on Bray-Curtis dissimilarities. Ordination was constrained by genotypes and conditions by soil batches, biological replicates and sequencing runs. Colours and shapes represent the genotypes and biological replicates, respectively. Variation explained by genotypes based on permutational analyses of variance (PERMANOVA; n = 999) is indicated at top-right. Asterisks indicate statistical significance based on PERMANOVA (α = 0.05). Trp, tryptophan; IAOx, indole-3-acetoaldoxime; IG, indole glucosinolates; GST, glutathione-*S*-transferase; SOT, sulfotransferase; UGT, uridine diphosphate-glycosyltransferase.

Figure 2. Root secretion of Trp-derived metabolites is partly dependent on PYK10 and BGLU21. (*A*) Sparse Partial Least Squares Discriminant Analysis plot of root-exuded metabolomic profiles. Colours and shapes represent the genotypes and biological replicates, respectively. (*B*) Venn diagrams representing the differentially accumulated metabolites in

801 *cyp79b2b3* and *pyk10bglu21* mutants compared to Col-0 for each biological replicate
802 (moderated *t* test; FDR ≤ 0.05 and |log fold change| ≥ 1.0).

803 **Figure 3. Compounds secreted into the rhizosphere in a PYK10- and BGLU21-dependent**
804 **manner have an impact on microbial community assembly in the soil environment.** Soils
805 were treated with root exudates (*A*) or root extracts (*B*) consecutively for 15 days with 2-day
806 intervals. Constrained PCoA plots are based on Bray-Curtis dissimilarities of bacterial (left) and
807 fungal (right) communities, and the ordination was constrained by genotypes and conditioned
808 by biological and technical replicates. The scatter plots show a comparison of changes in
809 relative abundance of ASVs (magenta) or families (green) in soils treated with mutant root
810 exudates/extracts compared to soils treated with Col-0 root exudates/extracts. Size
811 corresponds to their mean relative abundance in soils treated with Col-0 root exudates/extracts.
812
813 **Figure 4. Compounds secreted into the rhizosphere in a PYK10- and BGLU21-dependent**
814 **manner have a direct impact on bacterial community assembly.** (*A*) Schematic
815 representation of experiments using a bacterial SynCom composed of 171 root-derived and 29
816 soil-derived isolates. (*B*) Constrained PCoA analysis of bacterial communities in root exudates
817 from Col-0 (black), *pyk10bglu21* (blue) and *cyp79b2b3* (red) at 24 and 72 hours post inoculation
818 (hpi) using Bray-Curtis dissimilarities based on the relative abundance. Shapes correspond to
819 the individual replicates of root exudates. Ordination was constrained by genotypes and
820 conditioned by biological and technical replicates.
821
822 **Figure 5. ER bodies and Trp metabolism are needed for an appropriate accommodation**
823 **of endophytic fungi.** (*A*) Schematic representation of experimental setup using a set of
824 endophytic fungi isolated from healthy plant roots. (*B*) Representative images of plants
825 inoculated with fungi along with axenic control plants. (*C*) A phylogenetic tree of fungi used in

826 this study along with their impact on Col-0 growth compared to the axenic plants (left panel)
827 and the impact of *pyk10bglu21* and *cyp79b2b3* mutations on shoot growth with respect to Col-
828 0 plants inoculated with the same fungal strain. Marked with bold lines are FDR ≤ 0.05 and
829 |logFC| ≥ 0.5.
830
831 **Supplementary figure legends**
832 **Figure S1. Community shifts observed in the mutant roots compared to Col-0 roots**
833 **retained at the family level.** Constrained principal coordinates analysis (PCoA) of the bacterial
834 and fungal community structures in the roots of Col-0 as well as mutants impaired in ER body
835 formation (*nai1-1*), ER body-accumulating myrosinases (*pyk19bglu21*), IG biosynthesis
836 (*myb34/51/122*), and Trp metabolism (*cyp79b2b3*) based on Bray-Curtis dissimilarities
837 computed from the relative abundance aggregated at the family level. Ordination was
838 constrained by genotypes and conditions by soil batches, biological replicates and sequencing
839 runs. Colours and shapes represent the genotypes and biological replicates, respectively.
840 Variation explained by genotypes and respective *P* values based on permutational analyses of
841 variance (PERMANOVA; n = 999) are indicated at top-left.
842
843 **Figure S2. Similar effects of ER body pathway and Trp metabolism on root microbiota**
844 **community structure at the ASV level.** Comparison of $\log_2$-scale fold changes in relative
845 abundance of bacterial ASVs (A and B) and fungal ASVs (C and D) in rhizoplane (A and C) and
846 endosphere (B and D) fractions of mutants compared to respective Col-0. ASVs that are
847 consistently detected in all genotypes are marked with solid lines. Open and closed points
848 correspond to two independent soil batches. Pearson's correlation coefficients are indicated at
849 top-left.
850

Figure S3. Similar effects of ER body pathway and Trp metabolism on root microbiota community structure at the family level. Comparison of log_2-scale fold changes in relative abundance of bacterial ASVs (A and B) and fungal ASVs (C and D) aggregated at the family level in rhizoplane (A and C) and endosphere (B and D) fractions of mutants compared to respective Col-0. ASVs that are consistently detected in all genotypes are marked with solid lines. Open and closed points correspond to two independent soil batches. Pearson's correlation coefficients are indicated at top-left.

Figure S4. Several bacterial and fungal families are commonly enriched or depleted in mutant roots compared to wild-type roots. The dotted heatmap represents log_2-scale fold changes in relative abundance of bacterial (A) and fungal ASVs (B) aggregated at the family level in mutant roots compared to Col-0 roots. The mean aggregated relative abundance of each family across all genotypes in each soil batch is shown as a barplot.

Figure S5. Relative amounts of glucosinolates, auxin, and coumarins in the mutant root exudates. Relative abundance of metabolites in exudates normalized to Col-0 root exudates are shown as boxplots. Aliphatic (A–J), benzyl (K) and indole glucosinolates (L–N), as well as known indolic compounds (O and P) and coumarins (Q–S) are quantified based on either standards or KEGG annotation. Letters indicate statistical significance corresponding to ANOVA and post-hoc Tukey's HSD tests within each metabolite ($\alpha = 0.05$). Metabolites without statistical significance based on ANOVA are shown without letters. 9MSN, 9-methylsulfinylnonyl glucosinolate; 9MTN, 9-methylthiononyl glucosinolate; 5MTP, 5-methylthiopentyl glucosinolate; 8MSO, 8-methylsulfinyloctly glucosinolate; 3MSB, 3-methylsulfinylpropyl glucosinolate; 6MTH, 6-methylthiohexyl glucosinolate; 10MSD, 10-

876 methylsulfonyldecyl glucosinolate; 1MI3G, 1-methoxyindol-3-ylmethyl glucosinolate; 4MI3G, 4-
877 methoxyindol-3-ylmethyl glucosinolate; I3G, indol-3-ylmethyl glucosinolate; IAN, indole-3-
878 acetonitrile; IAA, indole-3-acetic acid.

879

880 **Figure S6. The relative abundance of microbes is different in the mutant root**
881 **compartment compared to the wild type**. The dotted heatmap represents log_2-scale fold
882 changes in relative abundance of bacterial (A) and fungal ASVs (B) aggregated at the family
883 level in soils treated with mutant root exudates or extracts compared to the soils treated with
884 Col-0 root exudates or extracts. The mean aggregated relative abundance of each family
885 across all genotypes in each treatment is shown as a barplot.

886

887 **Figure S7. Community dynamics and growth of individual microbes in a SynCom treated**
888 **with root exudates.** (A) The overall growth of the 200-member SynCom based on the
889 aggregated quantitative abundance (QA) of the strains relative to spiked-in DH5α. Top panels,
890 experiment 1; bottom panels, experiment 2. Left panels, low-titre inocula (OD_{600} = 0.005); right
891 panels, high-titre inocula (OD_{600} = 0.05). Colours represent the genotypes from which root
892 exudates were collected. (B) Constrained PCoA analysis of SynCom that compared community
893 structures when treated with the root exudates from the same genotype, based on Bray-Curtis
894 dissimilarities computed from relative abundances. Ordinations are constrained by the starting
895 titres and time points (represented by colours) and conditioned by technical and biological
896 replicates as well as independent batches of root exudate (represented by shapes). Arrows
897 indicate the community shift over the incubation period. Numbers on top indicate the overall
898 variance explained by the initial titre and the time points. (C) Heatmaps showing the taxonomy,
899 quantitative abundance relative to spiked-in DH5α and log2-scale fold change of QA (QA

logFC) in mutant root exudates compared to Col-0 root exudates. (D) Comparison of QA logFC in mutant exudates compared to Col-0 exudates of the strains whose mean QA is higher than 5. Strains whose growth is commonly promoted or suppressed in both mutant exudates are represented by green or magenta, respectively.

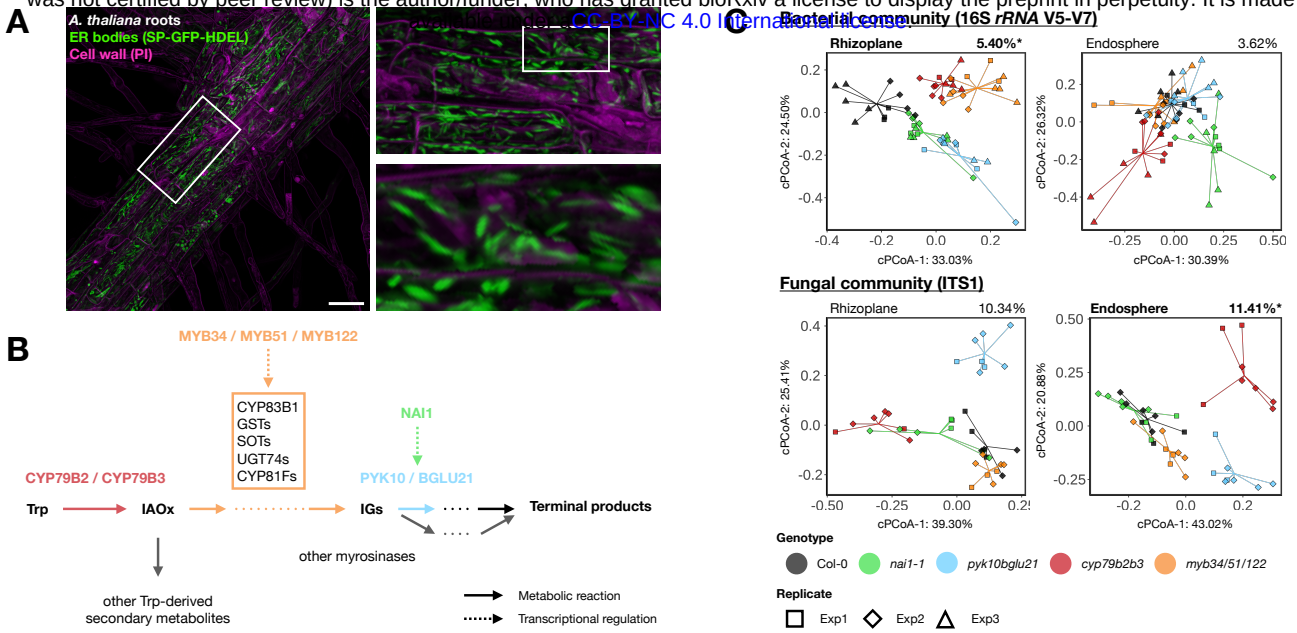

Figure 1. ER bodies and Trp metabolism play a role in root-associated microbiota assembly. (*A*) Roots of *A. thaliana* developing a large amount of ER bodies, visualized by ER-localized GFP (SP-GFP-HDEL). Cell wall was stained by propidium iodide. The bar corresponds to 50 mm. (*B*) Representation of IG biosynthetic and catabolic pathways. Arrows and dotted arrows indicate metabolic reactions and transcriptional regulation, respectively. (*C*) Constrained principal coordinates analysis (PCoA) of the bacterial and fungal community structures in the roots of Col-0 as well as mutants impaired in ER body formation (*nai1-1*), ER body-accumulating myrosinases (*pyk19bglu21*), IG biosynthesis (*myb34/51/122*), and Trp metabolism (*cyp79b2b3*) based on Bray-Curtis dissimilarities. Ordination was constrained by genotypes and conditions by soil batches, biological replicates and sequencing runs. Colours and shapes represent the genotypes and biological replicates, respectively. Variation explained by genotypes based on permutational analyses of variance (PERMANOVA; n = 999) is indicated at top-right. Asterisks indicate statistical significance based on PERMANOVA (α = 0.05). Trp, tryptophan; IAOx, indole-3-acetoaldoxime; IG, indole glucosinolates; GST, glutathione-*S*-transferase; SOT, sulfotransferase; UGT, uridine diphosphate-glycosyltransferase.

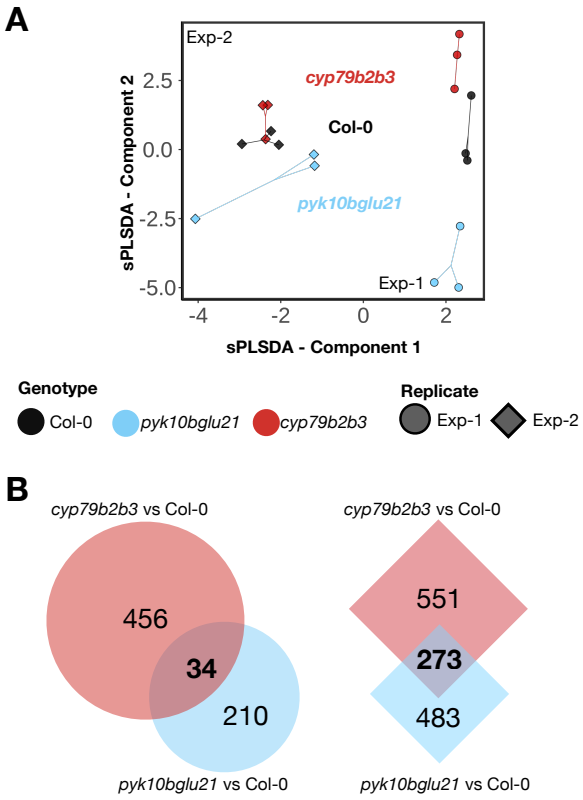

Figure 2. Root secretion of Trp-derived metabolites is partly dependent on PYK10 and BGLU21. (*A*) Sparse Partial Least Squares Discriminant Analysis plot of root-exuded metabolomic profiles. Colours and shapes represent the genotypes and biological replicates, respectively. (*B*) Venn diagrams representing the differentially accumulated metabolites in *cyp79b2b3* and *pyk10bglu21* mutants compared to Col-0 for each biological replicate (moderated *t* test; FDR ≤ 0.05 and llog fold changel ≥ 1.0).

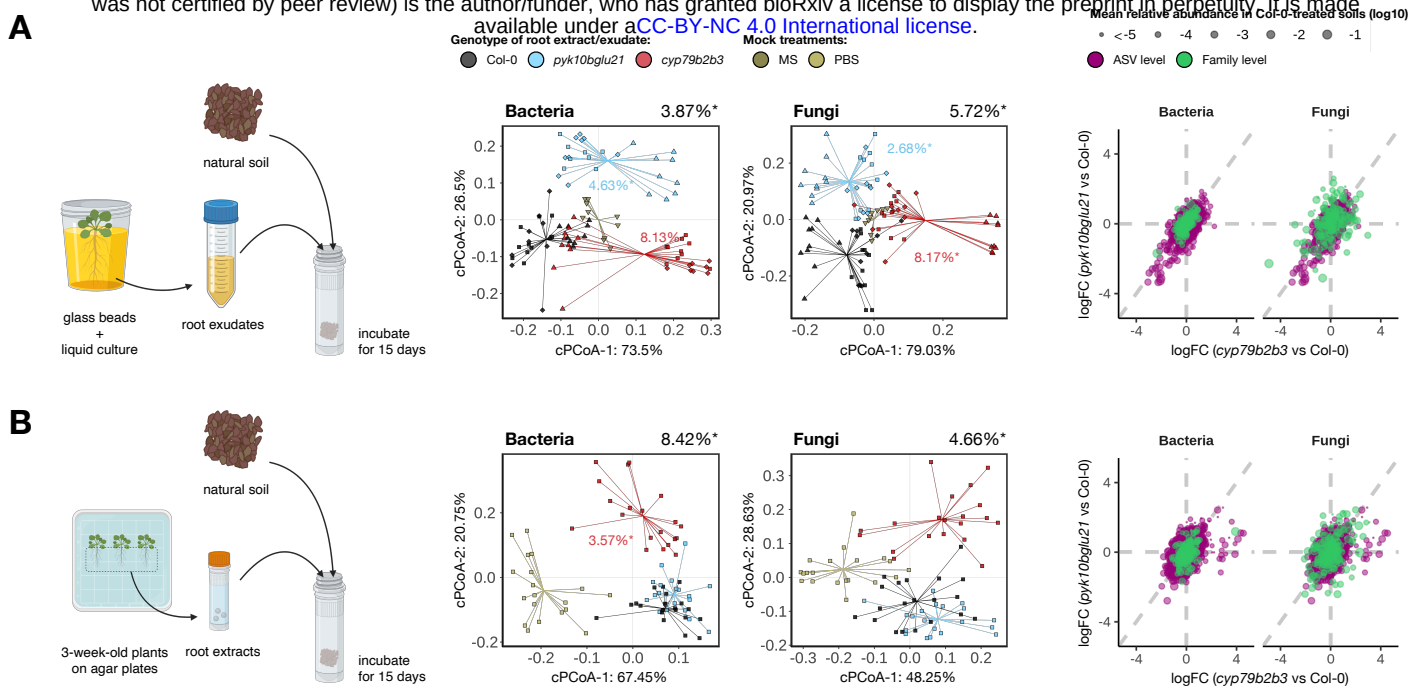

Figure 3. Compounds secreted into the rhizosphere in a PYK10- and BGLU21-dependent manner have an impact on microbial community assembly in the soil environment. Soils were treated with root exudates (*A*) or root extracts (*B*) consecutively for 15 days with 2-day intervals. Constrained PCoA plots are based on Bray-Curtis dissimilarities of bacterial (left) and fungal (right) communities, and the ordination was constrained by genotypes and conditioned by biological and technical replicates. The scatter plots show a comparison of changes in relative abundance of ASVs (magenta) or families (green) in soils treated with mutant root exudates/extracts compared to soils treated with Col-0 root exudates/extracts. Size corresponds to their mean relative abundance in soils treated with Col-0 root exudates/extracts.

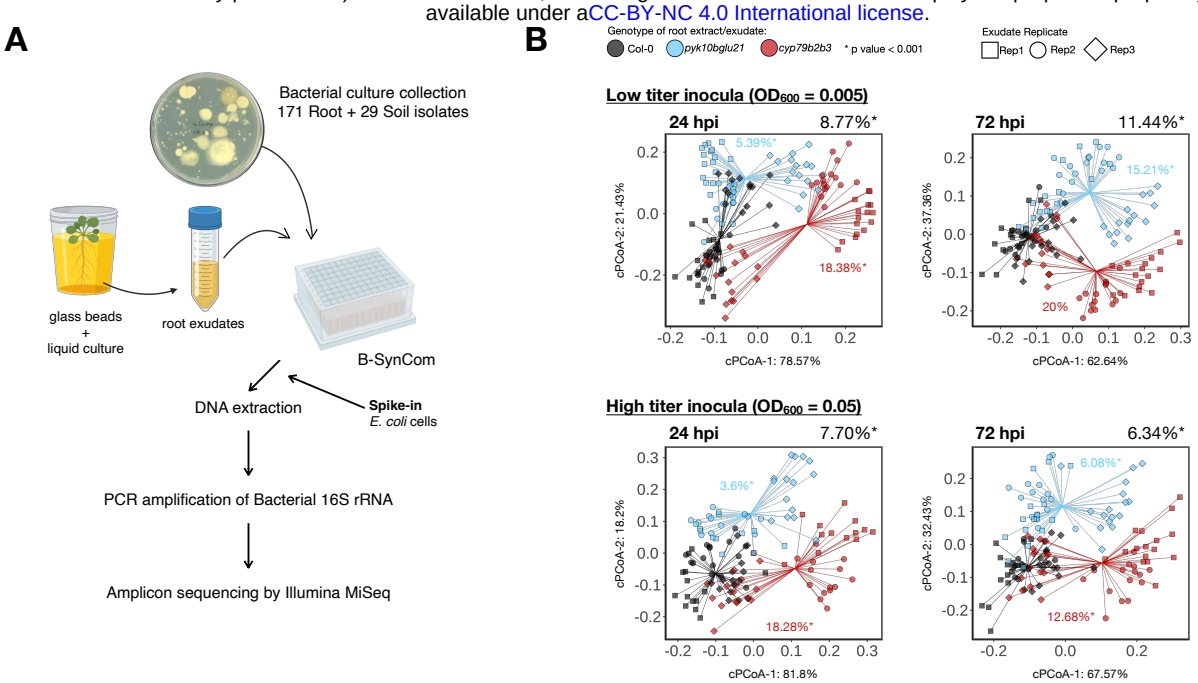

Figure 4. Compounds secreted into the rhizosphere in a PYK10- and BGLU21-dependent manner have a direct impact on bacterial community assembly. (*A*) Schematic representation of experiments using a bacterial SynCom composed of 171 root-derived and 29 soil-derived isolates. (*B*) Constrained PCoA analysis of bacterial communities in root exudates from Col-0 (black), *pyk10bglu21* (blue) and *cyp79b2b3* (red) at 24 and 72 hours post inoculation (hpi) using Bray-Curtis dissimilarities based on the relative abundance. Shapes correspond to the individual replicates of root exudates. Ordination was constrained by genotypes and conditioned by biological and technical replicates.

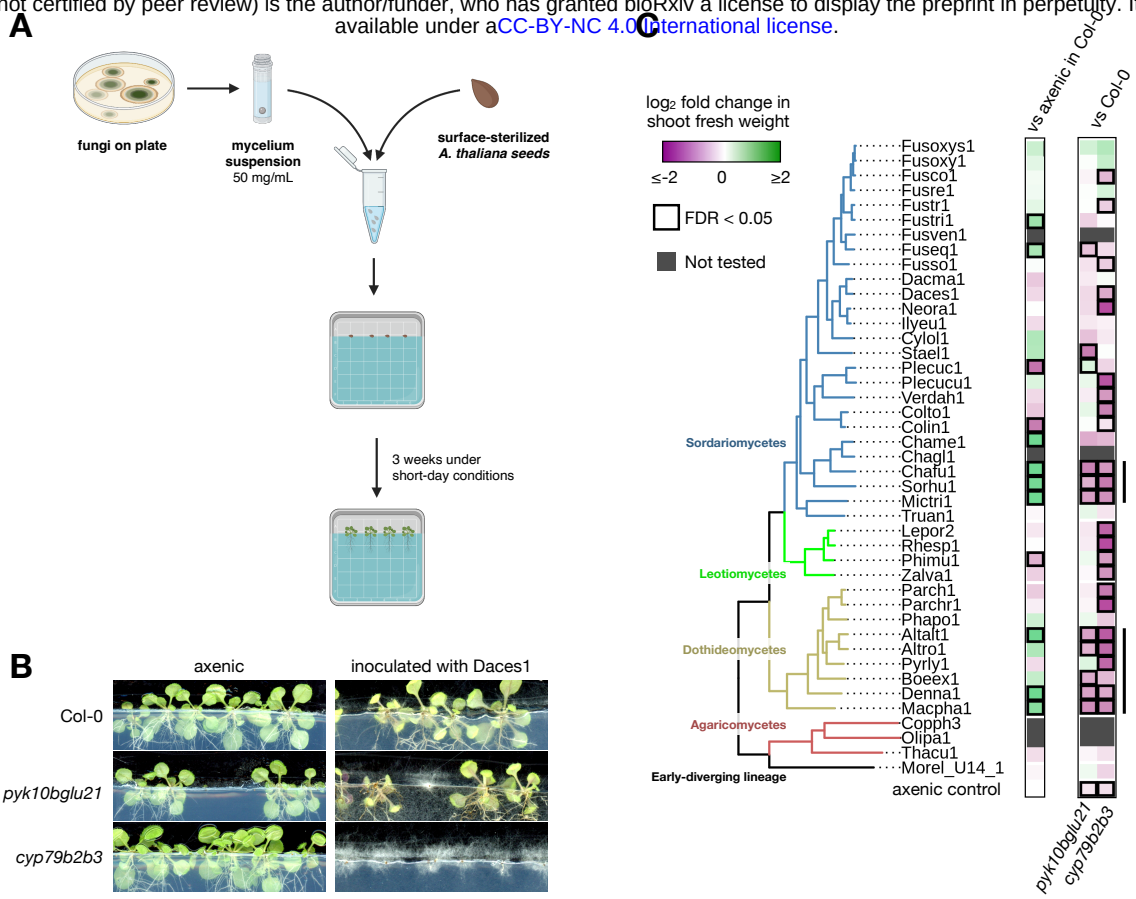

Figure 5. ER bodies and Trp metabolism are needed for an appropriate accommodation of endophytic fungi. (*A*) Schematic representation of experimental setup using a set of endophytic fungi isolated from healthy plant roots. (*B*) Representative images of plants inoculated with fungi along with axenic control plants. (*C*) A phylogenetic tree of fungi used in this study along with their impact on Col-0 growth compared to the axenic plants (left panel) and the impact of *pyk10bglu21* and *cyp79b2b3* mutations on shoot growth with respect to Col-0 plants inoculated with the same fungal strain. Marked with bold lines are FDR ≤ 0.05 and |logFC| ≥ 0.5.